NJC

Accepted Manuscript

This is an *Accepted Manuscript*, which has been through the Royal Society of Chemistry peer review process and has been accepted for publication.

Accepted Manuscripts are published online shortly after acceptance, before technical editing, formatting and proof reading. Using this free service, authors can make their results available to the community, in citable form, before we publish the edited article. We will replace this *Accepted Manuscript* with the edited and formatted *Advance Article* as soon as it is available.

You can find more information about *Accepted Manuscripts* in the Information for Authors.

Please note that technical editing may introduce minor changes to the text and/or graphics, which may alter content. The journal's standard Terms & Conditions and the Ethical guidelines still apply. In no event shall the Royal Society of Chemistry be held responsible for any errors or omissions in this *Accepted Manuscript* or any consequences arising from the use of any information it contains.

ROYAL SOCIETY OF CHEMISTRY

www.rsc.org/njc

Red lead degradation: monitoring of color change over time

Yang Zhao,[a] Yun Tang,[a] Tong Tong,[b] Zhijun Sun,[c] Zongren Yu,[c] Yixuan Zhu,[d] and Hua Tong[a*]

[a]College of Chemistry and Molecular Sciences, Wuhan University, Wuhan 430072, China

[b]Centre of Cultural Material Conservation, The University of Melbourne, Parkville VIC 3010，Australia

[c]Dunhuang Research Academy, Dunhuang 736200, China

[d]School of Remote Sensing and Information Engineering, Wuhan University, Wuhan 430072, China

[*]sem@whu.edu.cn

Abstract

Specimen of Chinese ancient pigment dating from the Song Dynasty (A.D. 960–A.D. 1279) as well as artificially aged red lead specimens were examined by scanning electron microscope, energy dispersive spectroscopy, X-ray photoelectron spectroscopy, X-ray diffraction, Raman spectroscopy and colorimeter. The aging tests simulating the weak acidic environment of the Mogao Grottoes were performed to investigate the aging mechanism for the purpose of assessing the level of red lead degradation in cases where the red lead was not mixed with other pigments. Hydrogen ions from the microbial metabolite and light were found to be the main deteriorating factors leading to red lead discoloration. Hydrogen ions led to a disproportionation reaction of red lead, and light oxidized red lead to form lead dioxide. In addition, the chemical composition of the artificially aged red lead specimens was fitted functions with aging time and chromatic values, respectively. Based on these functions, the mechanism and process of red lead discoloration could be visually described.

Key words: ancient pigment, red lead, artificial aging, discoloration mechanism, function fitting.

1 Introduction

Red lead is considered to be one of the earliest manufactured pigments in Chinese art history[1] and has been used worldwide in murals,[2-8] polychrome sculptures,[9-11] manuscript illumination[12,13] and canvas paintings.[14,15] Red lead (characteristic bands of Raman spectrum at 548, 390, 223, 149 and 122 cm^{-1})[13] can be used as a single pigment or mixed with other pigments such as white lead, vermilion, orpiment, and red ochre.[16] In particular, the combination of red lead and white lead to produce flesh tones is commonly seen on paintings from the Mogao Grottoes[17] which is located in Dunhuang of China. Due to the atmospheric pressure from Mongolia, Dunhuang has a typical continental desert climate, which shows some remarkable characteristics of hot summer, cold winter, strong wind, sandy climate, less precipitation and low temperature. In this region, the temperature ranges from -21.5 ^{0}C to 40.6 ^{0}C, and the mean annual temperature is 10.6 ^{0}C. The average annual precipitation is 23.2 mm, the relative humidity is 32.2% RH, and the annual sunshine hours are 2962.5 h.[18]

The Mogao Grottoes (366 A.D.) represent the peak of Chinese ancient murals and sculptures. The murals of the Mogao Grottoes could be divided into three layers. The first layer was prepared by mixing wheat straw and silty soil, then the mixture was brushed on the rock to form a flat surface. The thickness of the first layer was about 2–5 cm. After that, the fine silt from the riverbed of Daquan River was brushed on the surface of this layer, and the thickness of the second layer was about 0.3–0.5 cm. Finally, the surface was covered with gypsum, lime or kaolin to be used for painting.[19] High red lead content has been identified in the pigments used on the cassocks and Buddha faces in the murals from the Mogao Grottoes.

During the aging process, red lead pigment undergoes various types of discoloration. In some rare cases, the color of red lead turns lighter,[20] which causes significant fading in the surrounding areas of the paintings. However, in most cases, most red lead alterations can be described in terms of either darkening or blackening. Such phenomena are due to the transformation of red lead into secondary phases. Black lead dioxide is generally considered to be the product of the phase transition of red lead.[21] The murals in Mogao Grottoes are facing the same problems as well, as shown in Fig. 1. Almost all the red and flesh tones have transformed into dark or black lead dioxide,[22] which compromises the decorative and artistic value of the murals. There is no definitive explanation for red lead discoloration because light,[23-25] humidity,[26,27] fungal contamination,[28,29] H_2S,[30,31] interaction of lead-based pigments with sulfur-containing pigments[32,33] and hydrogen ions[20,34] may all potentially be responsible for darkening of red lead. Therefore, it is important to investigate the deterioration mechanism of red lead darkening on the murals of the Mogao Grottoes for preservation and restoration purposes.

Fig. 1 Sampling area of Cave 230 in the Mogao Grottoes.

In the Mogao Grottoes, many species of fungi were considered to have an effect on the decomposition of bone glue which acted as a binder for pigments. Since bone glue was decomposed, red lead on the murals lost the protective effect that the bone glue had on it.[35] On the other hand, oxalate was also generally found in many color–changed murals of the Mogao Grottoes. As the microbial metabolite, it would react with red lead slowly. Then the

crystals of red lead were damaged to form into the degradation products. In addition, the oxalate could also react with the calcium salt from the murals to form the calcium oxalate.[1] To assess the extent of red lead degradation, aging tests simulating the weak acidic environment of the Mogao Grottoes were performed to study the discoloration mechanism. The chemical composition and chromatic value of the aged samples were determined by this process. The aging mechanism was analyzed from the aspects of microstructure, composition of inorganic elements, phase change, molecular fingerprint information, and the visible spectrum. Then the chemical composition of the artificial aged red lead specimens was fitted functions with the aging time and the chromatic values, respectively. Based on these functional relationships, the mechanism and process of red lead discoloration could be visually described.

2 Materials and methods

2.1 Materials

An ancient black pigment sample (Cave 230-41) dating back to the Song Dynasty (A.D. 960-A.D. 1279) from the Mogao Grottoes was supplied by the Dunhuang Research Academy (Dunhuang, China). The red lead (Pb_3O_4, analytical purity grade) was purchased from Sinopharm Chemical Reagent Co. (Shanghai, China).

2.2 Acid mist aging

When the samples were prepared, 1 g of red lead was tiled on the bottom of the beaker (50 ml), then a group of 10 red lead samples were placed in the salt spray test chamber. The relative humidity was set at 85±5% RH, the pH of acid mist was controlled at 5, and the temperature was set at 25ºC. One red lead sample was taken out from the salt spray test chamber every 3 days, and each red lead sample was washed three times with ultrapure water and dried in the oven at 60ºC for 12 hours. The aged samples were denoted as 3 d, 6 d, 9 d…27 d, 30 d, respectively.

2.3 Ultraviolet (UV) light aging

The fresh red lead samples were exposed to Ultra-violet radiation lamp for 15 d at 25ºC. The relative humidity was set at 40% RH, the intensity of irradiation was 30 mW/cm^2, and the illuminant was a 250 W high pressure mercury lamp with the continuous transmitting wavelengths ranging from 200 to 1400 nm in which 365 nm is the dominant transmitting wavelength.

2.4 Characterization

Scanning Electron Microscope (SEM) images of the ancient pigment sample and the acid mist aged samples were observed with a Quanta 200 Scanning Electron Microscope (FEI, Netherlands) at 30 keV accelerating voltage. Semiquantitative elemental analysis of the ancient pigment sample and the acid mist aged samples was obtained by SEM-associated Energy Dispersive Spectroscopy (EDS) area analysis (EDAX GENSIS, AMETEK, USA). X-ray diffraction (XRD) of the acid mist aged samples was performed by an Xpert Powder diffractometer (PANalytical, Netherlands) with Cu Kα radiation from a source operated at 40 kV and 40 mA. X-ray Photoelectron Spectroscopy (XPS) (ESCALAB 250Xi, Thermo Fisher, USA) was performed on the ancient pigment sample and all the aged samples to obtain the information about the valence of the lead element. Raman spectroscopy was carried out on a Raman microspectrometer (LabRam HR800, Jobin Yvon, France) with the 632.8 nm line of a He–Ne laser as excitation source. The color change of the acid mist aged samples was measured by using a recording colorimeter (CM-2600d, Konica Minolta, Japan). The reflectance data were recorded in the range of 360-740 nm at 10 nm increment. The chosen optics aperture size of the spectrophotometer was 8 mm.

3 Results and discussion

3.1 Chromaticity coordinates

Tristimulus coordinates were determined for both the pure red lead and the samples aged in acid mist using the CIE1931 standard observer functions and the D_{65} standard illuminant source. The CIE chromaticity coordinates for

the specimens were converted to CIE1976L*a*b* by software in the colorimeter. The colors of the specimens, which varied from red to black, were observed by the naked eye (Fig. 2a). The spectral reflectance curves of the specimens are shown in Fig. 2b. The CIE1976L*a*b* chromaticity coordinates for the specimens are given in Table 1. The values of L* ranged from 61.36 to 27.63, the values of a* denoting the red /green chromaticity coordinate ranged from 52.79 to 4.04, and the values of b* denoting the yellow/blue chromaticity coordinate ranged from 63.81 to 2.71. The real color information obtained provided the basis for studying the discoloration process, and the CIE1976L*a*b* chromaticity coordinate was used to describe the real color information.

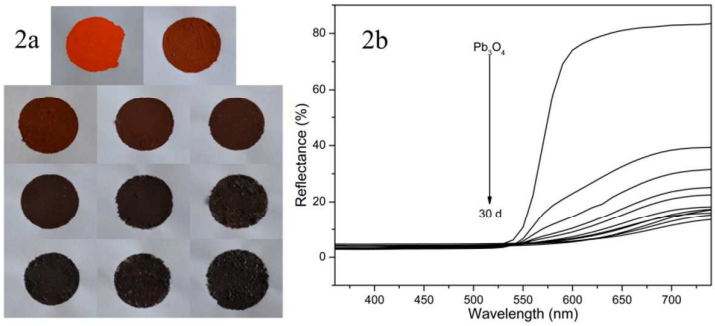

Fig. 2 (a) Colors of pure red lead and 10 samples aged in acid mist; (b) spectral reflectance curves for pure red lead and 10 samples aged in acid mist.

Table 1 CIE 1976 L*a*b* chromaticity coordinates for pure red lead and 10 samples aged in acid mist.

Sample	L*	a*	b*	Sample	L*	a*	b*
0 d	61.36	52.79	63.81	18 d	27.83	8.98	7.16
3 d	40.27	31.75	34.83	21 d	27.80	7.76	6.09
6 d	34.48	24.49	24.69	24 d	26.92	5.68	4.07
9 d	30.85	18.53	17.86	27 d	25.70	7.03	5.31
12 d	29.67	15.64	14.57	30 d	27.63	4.04	2.71
15 d	27.87	11.85	10.31				

3.2 Morphology

The microstructure of the pigment samples can be directly observed from the SEM images. It was observed that the ancient pigment sample consisted of irregular particles with a particle size of 100 μm (Fig. 3a). The particle size of the ancient pigment sample was larger than that of the aged red lead samples because the ancient pigment sample included layers of ground plaster adhering to the back. The surface was covered with tiny particles, which were probably foreign materials from environmental contamination. According to the results of EDS, the tiny particles were composed of Si, Ca, Mg, and Al. As shown in Fig. 3b, the red lead sample without aging had an irregular sheet structure with a particle size of 5 μm and was also covered with tiny contamination particles. The particle size of the acid mist aged samples decreased as the aging time increased (Figs. 3c–3l). In the later stages of the aging process, particle aggregation could be observed, and particle surface morphology became similar to the ancient pigment sample. Due to the close relationship between particle size and color, the reduced particle size of the red lead had an influence on discoloration.

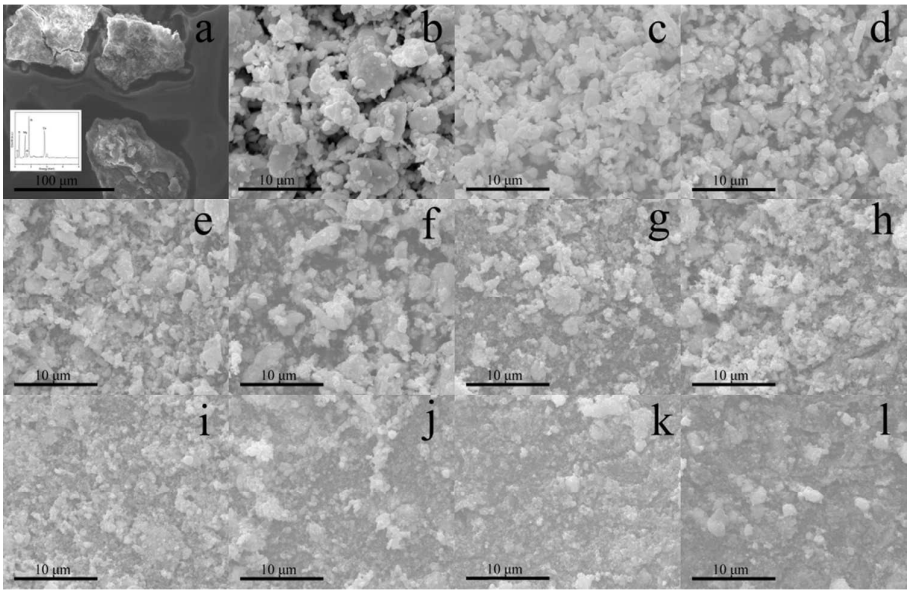

Fig. 3 SEM images of the ancient black pigment sample and the acid mist aged samples: (a) ancient black pigment sample, (b) pure red lead sample, (c) 3 d sample, (d) 6 d sample, (e) 9 d sample, (f) 12 d sample, (g) 15 d sample, (h) 18 d sample, (i) 21 d sample, (j) 24 d sample, (k) 27 d sample, and (l) 30 d sample.

3.3 Composition of inorganic elements

The ancient pigment sample was shown to be composed of elements Pb, Ca, Si, Mg, and Al using EDS. Therefore, it was reasonable to conclude that the sample was composed of lead-based pigment, with the other elements probably coming from the cave environment (Fig. 4a). Because the ancient pigment sample was black, it was tentatively inferred that the red lead had turned into lead dioxide through a phase transition.

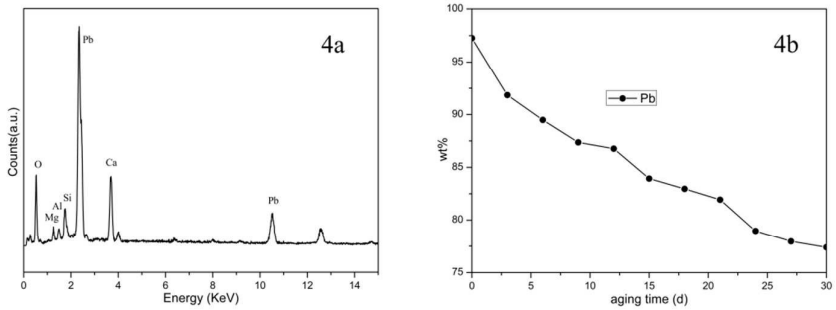

Fig. 4 (a) EDS result for the ancient black pigment sample and (b) lead content of the acid mist aged samples obtained by EDS.

In an acidic environment with high humidity, red lead, as a mixed–valence compound, forms lead dioxide and Pb^{2+} ions[20]:

$$Pb_3O_4+4H^+ \rightarrow PbO_2+2Pb^{2+}+2H_2O.$$

The mechanism of this chemical reaction is illustrated in Fig. 5. By the action of hydrogen ions, the Pb–O bonds in red lead were broken, forming Pb^{4+}, Pb^{2+}, and O^{2-}. Pb^{4+} then reacted with O^{2-} to form lead dioxide, H^+ reacted with the rest of the O^{2-} to form water, and Pb^{2+} may have reacted with sulfate, carbonate and chloride ions to form the corresponding salts.

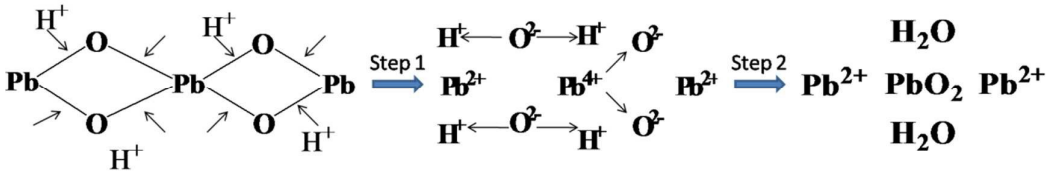

Fig. 5 Discoloration mechanism of red lead in an acidic environment

As illustrated in Fig. 4b, the lead content of the acid mist aged samples gradually decreased as aging time increased. The reason for the decrease in lead content in the acid mist aged samples was probably that the Pb^{2+} ions that would have formed the corresponding salts were washed away by ultrapure water. In the actual cave environment, the Pb^{2+} ions would form the corresponding soluble salts and be transported into the plaster layers with water from the cave environment.

3.4 Crystal structure

XRD results demonstrated that the aging product of the red lead during the artificial aging process was lead dioxide. As illustrated in Fig. 6, the typical diffraction pattern of pure red lead is represented by the peaks at 26.3º, 30.7º, and 32.1º, which represent crystal planes (211), (112), and (310) respectively. For the sample aged for 30 days, the diffraction peaks at 25.4º, 32.0º, and 49.1º represent crystal planes (110), (101), and (211), which indicate the presence of lead dioxide.

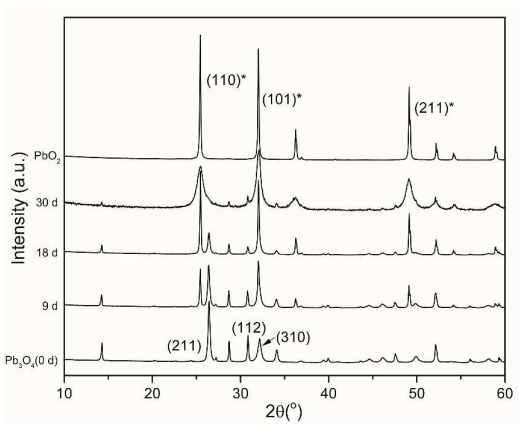

Fig. 6 XRD patterns of pure red lead, lead dioxide, and the samples aged in acid mist.

The coexistence of red lead and lead dioxide could be observed in the XRD diagrams for the acid mist aged samples, aside from the sample aged for 30 days. In addition, the intensities of the red lead peaks decreased, whereas the intensities of the lead dioxide peaks increased through the aging process. The change in the intensities of the diffraction peaks indicated the phase transition of red lead, during which the original crystal structure was replaced by the crystal structure of lead dioxide.

3.5 Valence state analysis and quantitative calculation

To verify the hypothesis that lead dioxide was the product of the aging of red lead during the natural aging process, the transition state of Pb was investigated by XPS analysis (Fig. 7). The high–resolution XPS spectrum was analyzed by scanning with the following results: the binding energy for the Pb 4f region was around 140 eV; the Pb 4f spectrum was in the range of 134–148 eV with two peaks, which were attributable to Pb $4f_{5/2}$ and Pb $4f_{7/2}$ respectively. The peaks appearing at 137.0 and 141.9 eV corresponded to the Pb $4f_{7/2}$ and Pb $4f_{5/2}$ states, indicating the presence of Pb^{4+} (Fig. 7a).

The samples aged by acid mist were also investigated by XPS. Figure 7b shows the XPS spectra of the sample aged for 30 days. In the high–resolution XPS spectrum, the peak at 137.0 eV indicates that the valence state of Pb is +4. Therefore, it was reasonable to conclude that the aging products of both the natural and artificial aging

processes were lead dioxide, which further confirmed the inference made from the EDS results.

Some small black particles were observed in the red lead samples aged by exposure to the UV lamp for 15 days. These small black particles were collected by precision tweezers for XPS testing. The XPS results also showed that the UV-aged product was lead dioxide (Fig. 7c). The electrons in the 6s orbit of the Pb atom were attracted strongly by the atomic nucleus due to the penetration effect; however, photon energy could eject the lone pair of electrons in the 6s orbit, subsequently transforming the Pb^{2+} ions into Pb^{4+} ions. Red lead became lead dioxide by a photo-oxidation process as the Pb^{2+} ions were oxidized into Pb^{4+} ions:

3.5.1 $Pb_3O_4+O_2 \xrightarrow{UV} 3PbO_2$ ($\Delta_rG_m^\theta$= -463 kJ/mol, E^θ=1.20 V)

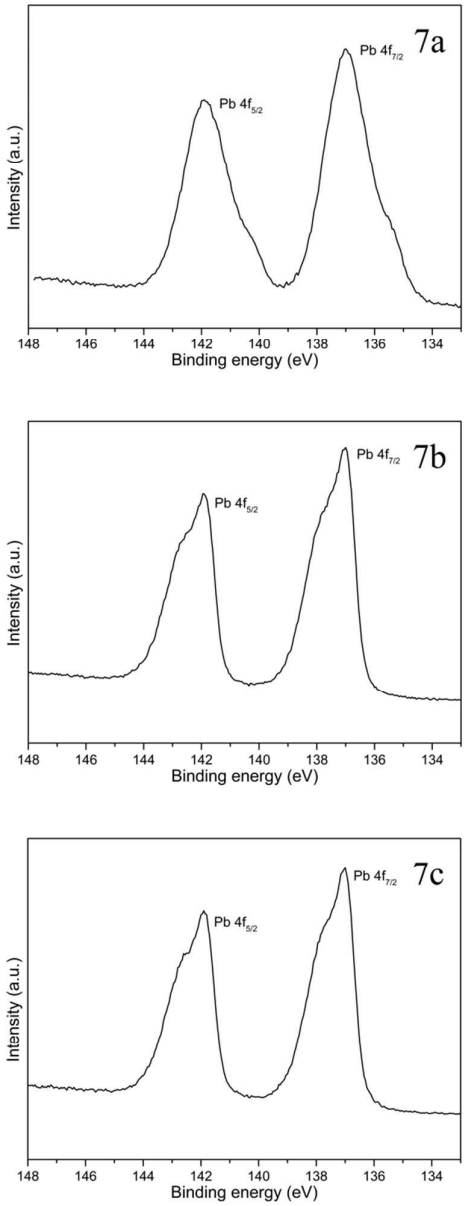

Fig. 7 High–resolution XPS spectra for (a) Pb 4f of the ancient black pigment sample, (b) Pb 4f of the sample aged for 30 days in acid mist, and (c) Pb 4f of the light–aged sample.

Based on the XPS spectra, the relative contents of red lead and lead dioxide were measured. Figure 8 shows the

XPS spectra of pure red lead without the aging process and of the 10 samples aged in acid mist. The peak at 137.7 eV in the XPS spectrum of pure red lead indicates that the valence state of Pb is +8/3. The sample aged for 30 days was determined to be pure lead dioxide because only one peak appears at 137.0 eV. Two peaks appear at 137.0 eV and 137.7 eV in all other XPS spectra, indicating the existence of both lead dioxide and red lead. The XPS spectra of the pure red lead and the sample aged for 30 days were used as standards to fit the rest of the spectra by nonlinear least square fitting (NLLSF). The relative contents of red lead and lead dioxide could be determined according to the participation rates of the two standards in the fitting (Table 2). As shown in Table 2, lead dioxide content increased with aging time.

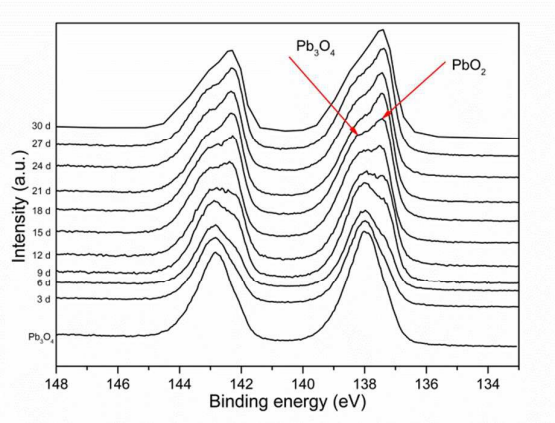

Fig. 8 High–resolution XPS spectra for Pb 4f of pure red lead and the acid mist aged samples.

Table 2 Contents of red lead and lead dioxide for the pure red lead and for the 10 samples aged in acid mist.

Time (d)	0	3	6	9	12	15	18	21	24	27	30
Pb_3O_4%	100	98.2	94.62	78.18	50.83	35.34	26.41	14.67	3.48	2	0
PbO_2%	0	1.8	5.38	21.82	49.17	64.66	73.79	85.33	96.52	98	100

3.6 Raman spectroscopy

For the molecular fingerprint information of the degradation products, Raman spectra were acquired from the ancient pigment sample and the sample aged for 30 days. As described earlier, lead dioxide showed a broad intense band at 515 cm^{-1}, and weak bands at 424 cm^{-1} and 653 cm^{-1}.[13] In the Fig. 9, the main bands of the sample aged for 30 days were in the range of 400-700 cm^{-1} with three peaks, corresponding to the main spectral features of lead dioxide. Due to the presence of the foreign materials and plaster ground layers, the intense band at 515 cm^{-1} could be observed, but the weak bands at 424 cm^{-1} and 653 cm^{-1} were not obvious in the Raman spectrum of the ancient pigment sample.

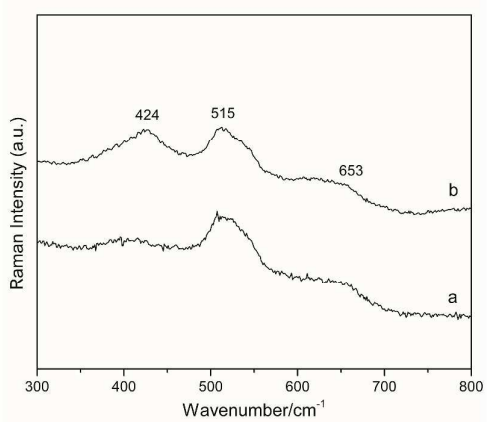

Fig. 9 Raman spectra of (a) the ancient pigment sample and (b) the sample aged for 30 days.

3.7 Function fitting

Chemical composition is the basis of substance color and also an important variable in the aging process. Therefore, the chemical composition obtained by XPS could be used as a link between color and aging time. In Fig. 10a, a functional relationship between aging time and chemical composition was obtained through nonlinear fitting and was defined as the time function. Meanwhile the functional relationships were fitted by the chemical composition with the values of L*, a*, and b*, respectively, and these functional relationships were defined as the color functions (Figs. 10b–10d). The corresponding time function and color functions were as follows:

Time function (t=aging time, X=lead dioxide content):

3.7.1 $X=-7.78422+108.04366/\{1+10^{[0.10743*(12.47903-t)]}\}$ (DoseResp).

Color functions (x=lead dioxide content, $Y_L=L^*$, $Y_a=a^*$, $Y_b=b^*$):

3.7.2 $Y_L=38.03779-2.39894ln(x-1.40246)$ (Log3P1).

3.7.3 $Y_a=36.46957-6.36044ln(x+0.07729)$ (Log3P1).

3.7.4 $Y_b=39.14834-7.33949ln(x+0.03476)$ (Log3P1).

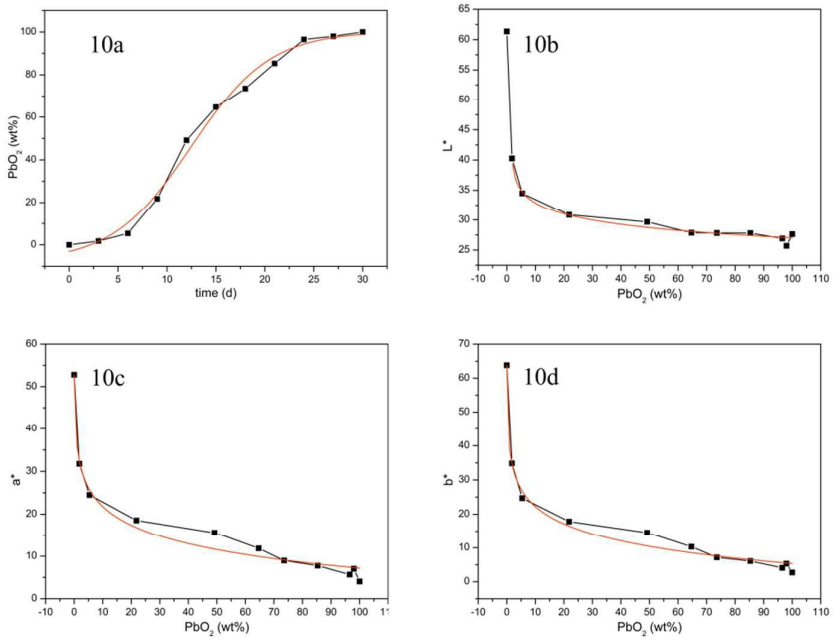

Fig. 10 (a) Time function was fitted by aging time with chemical composition and color functions were fitted by chemical composition with the values of (b) L*, (c) a*, (d) b*, respectively.

Based on the time and color functions, the mechanism and process of red lead discoloration could be described. Because the color state of red lead at each point in time could also be calculated, the level of red lead degradation could be assessed at the same time, provided that the red lead was not mixed with other pigments.

3.8 Discoloration process of red lead in the Mogao Grottoes

In the cave environment of the Mogao Grottoes, hydrogen ions were the main factor leading to discoloration, with light playing a supplementary role because it was weak in the cave. In addition, the sources of hydrogen ions were assumed to be from the air and from microorganisms. When the cave was maintained at high relative humidity, CO_2 could dissolve in the water to form carbonic acid. It was also possible that the microbial metabolites contained organic acids such as oxalate[1]. Therefore, the fact that the humid atmosphere and microorganism contamination caused discoloration of red lead could also be attributed to the abundant hydrogen ions in the surroundings.

4 Conclusions

The chemical compositions of an ancient pigment specimen that was naturally aged and the aging products from artificially aged pigment specimens were analyzed in this research. Lead dioxide was determined to be the main constituent of all the aged pigment specimens. Based on the integrated characterization of the naturally and artificially aged pigment specimens, a red lead discoloration mechanism was investigated and proposed. Hydrogen ions and light were found to be the cause of red lead discoloration. Hydrogen ions induced disproportionation reaction with red lead, which is a mixed–valence compound, leading to formation of Pb^{2+} and Pb^{4+} ions. Pb^{2+} ions were then consumed in the form of salts, and Pb^{4+} ions could form lead dioxide, leading to discoloration of the murals. Red lead can also be oxidized and form lead dioxide as photons excite the electrons in the 6s orbit of the Pb atom. Time and color functions were used to describe the mechanism and process of red lead discoloration, and the color states of red lead at each point in time were also obtained using the functions. Based on these results, the extent of red lead degradation could be assessed.

Acknowledgements

Financial support of this research from the National Basic Research Program of China (973 Program) (2012CB725300) is gratefully acknowledged.

Notes and references

1 Q. P. Feng, X. J. Zhang and X. J. Ma, *J. Gen. Appl. Microbiol.*, 1999, **45**, 85-88.

2 M. Del Monte, P. Ausset and R. Lefevre, *Archaeometry*, 1998, **40**, 403-412.

3 H. G. Edwards, D. W. Farwell, E. M. Newton and F. R. Perez, *Analyst*, 1999, **124**, 1323-1326.

4 S. Bruni, F. Cariati, F. Casadio and V. Guglielmi, *J.Cult. Herit.*, 2001, **2**, 291-296.

5 A. Doménech-Carbó, M. Doménech-Carbó, M. Moya-Moreno, J. Gimeno-Adelantado and F. Bosch-Reig, *Anal. Chim. Acta*, 2000, **407**, 275-289.

6 M. Pérez-Alonso, K. Castro, M. Alvarez and J. Madariaga, *Anal. Chim. Acta*, 2004, **524**, 379-389.

7 A. Perardi, L. Appolonia and P. Mirti, *Anal. Chim. Acta*, 2003, **480**, 317-325.

8 J. M. Bayne and I. S. Butler, *New J. Chem.*, 2013, **37**, 3833-3839.

9 O. Agarwal, *Stud. Conserv.*, 1971, **16**, 56-68.

10 M. Franquelo, A. Duran, J. Castaing, D. Arquillo and J. Perez-Rodriguez, *Talanta*, 2012, **89**, 462-469.

11 A. Doménech-Carbó, M. T. Doménech-Carbó and X. Mas-Barberá, *Talanta*, 2007, **71**, 1569-1579.

12 P. Vandenabeele, B. Wehling, L. Moens, B. Dekeyzer, B. Cardon, A. von Bohlen and R. Klockenkämper, *Analyst*, 1999, **124**, 169-172.

13 C. Miguel, A. Claro, A. P. Gonçalves, V. S. Muralha and M. J. Melo, *J. Raman Spectrosc.*, 2009, **40**, 1966-1973.

14 R. J. Clark and P. J. Gibbs, *J. Archaeol. Sci.*, 1998, **25**, 621-629.

15 S. Bruni, F. Cariati, F. Casadio and L. Toniolo, *Spectrochim. Acta A*, 1999, **55**, 1371-1377.

16 R. J. Clark and S. Mirabaud, *J. Raman Spectrosc.*, 2006, **37**, 235-239.

17 Y. M. Tang and R. T. Sun, *Dunhuang Research*, 1988, **3**, 18-27. (In Chinese)

18 W. F. Wang, T. Wang, Z. B. Shen, J. P. Xie and J. Xing, *Plateau Meteorology*, 2006, **1**: 164-168. (In Chinese)

19 L.Y. Zhao, Y. F. Li, Z. R. Yu and Z. X. Li, *Dunhuang Research*, 2005, **4**: 75-82. (In Chinese)

20 S. Aze, J.-M. Vallet, V. Detalle, O. Grauby and A. Baronnet, *Phase Transit.*, 2008, **81**, 145-154.

21 S. Aze, J.-M. Vallet, M. Pomey, A. Baronnet and O. Grauby, *Eur. J. Mineral.*, 2007, **19**, 883-890.

22 R. J. Wu, *Dunhuang Research*, 2003, **5**: 44-50. (In Chinese)

23 S. Daniilia, S. Sotiropoulou, D. Bikiaris, C. Salpistis, G. Karagiannis, Y. Chryssoulakis, B. A. Price and J. H. Carlson, *J. Cult. Herit.*, 2000, **1**, 91-110.

24 T. Kenjo and K. Toisi, *Shikizai Kyokaishi*, 1964, **37**, 133-137.

25 I. Hwang, M. Inaba and R. Sugisita, *Scientific Papers on Japanese Antiques and Art Crafts*, 1993, 10-19.

26 S. Giovannoni, M. Matteini and A. Moles, *Stud. Conserv.*, 1990, **35**, 21-25.

27 J. P. Petushkova and N. N. Lyalikova, *Stud. Conserv.*, 1986, **31**, 65-69.

28 M. Fomina, J. Charnock, A. D. Bowen and G. M. Gadd, *Environ. Microbiol.*, 2007, **9**, 308-321.

29 W. Wang, X. Ma, Y. Ma, L. Mao, F. Wu, X. Ma, L. An and H. Feng, *Int. Biodeter. Biodegr.*, 2010, **64**, 461-466.

30 G. D. Smith and R. J. Clark, *J. Cult. Herit.*, 2002, **3**, 101-105.

31 O. Ciferri, *Appl. Environ. Microb.*, 1999, **65**, 879-885.

32 C. S. Smith and J. G. Hawthorne, *Transactions of the American Philosophical Society*, 1974, 1-128.

33 F. Rull Perez, H. Edwards, A. Rivas and L. Drummond, *J. Raman spectrosc.*, 1999, **30**, 301-305.

34 E. Kotulanová, P. Bezdička, D. Hradil, J. Hradilová, S. Švarcová and T. Grygar, *J. Cult. Herit.*, 2009, **10**, 367-378.

35 Q. P. Feng, X. J. Zhang, X. J. Ma and L. Yang, *Acta Microbiologica Sinica*, 1998, **5**: 365-370. (In Chinese)

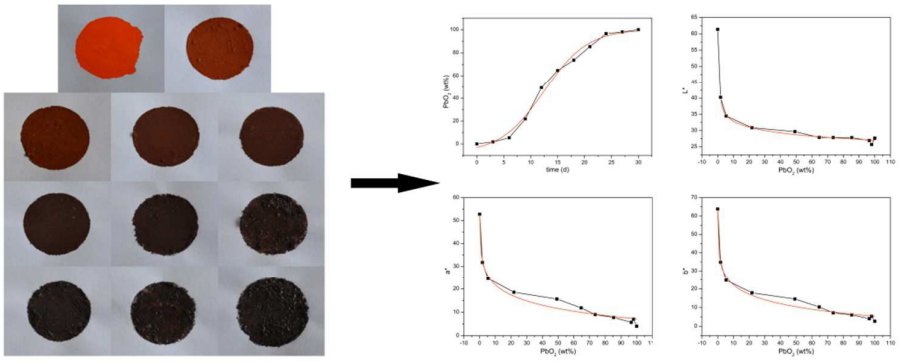

Time and color functions indicated the mechanism and process of red lead discoloration.